Resonant Raman scattering in the II-IV semiconductors Mg_2Si, Mg_2Ge, and Mg_2Sn

Seinosuke Onari* and Manuel Cardona
Max-Planck-Institut für Festkörperforschung, Stuttgart, Federal Republic of Germany
(Received 1 April 1976)

First- and second-order resonant Raman scattering from Mg_2Si, Mg_2Ge, and Mg_2Sn were measured with laser frequencies covering the E_0 and E_1 gaps for Mg_2Si, the E_1 gap for Mg_2Ge, and the E_1 and X gaps for Mg_2Sn. Each component of the Raman tensor is separated using polarized light. The resonance of the Raman allowed F_{2g} phonon for these three materials near the E_1 and $E_1+\Delta_1$ gaps is well described by three band terms in the dielectric theory of the Raman tensor. The resonance of the F_{2g} phonon near the E_0 gap of Mg_2Si was observed as a shoulder of the strongly resonating E_1 gap. The observed resonance intensity is about one-half the value expected from $|d\epsilon/d\omega|^2$ when this function is fitted to the maximum of the E_1 resonance. A pseudopotential calculation is presented, showing that the corresponding deformation potential (7.5 eV) is small. The resonance in the X-gap region for Mg_2Sn is found to be analogous to that of the E_1 gap. The F_{2g} allowed phonon resonates broadly and weakly; however, Fröhlich-interaction-induced F_{1u}(LO) and its overtone resonate sharply and show structure due to the spin-orbit splitting of the $X_{5'}$ valence band. The spin-orbit splittings observed in the resonances at E_1 gaps are 0.14 eV for Mg_2Ge and 0.27 eV for Mg_2Sn; at the X gap the splitting for Mg_2Sn is 0.14 eV. The deformation potentials involved in the several resonances observed are discussed and an attempt to determine their relative values is made. The forbidden F_{1u}(LO) and its overtone resonate very sharply at the E_1, $E_1+\Delta_1$, and X gaps: These resonances are well described by the second derivative of the dielectric constants $|d^2\epsilon/d\omega^2|^2$ and are strongly polarized in parallel-parallel scattering configurations. Sharp structure due to $F_{2g}+F_{1u}$(LO) combination of phonons is also observed; it resonates in a way analogous to the forbidden F_{1u}(LO) phonon. These characteristic features suggest that the normally forbidden F_{1u}(LO) and its overtone for the materials investigated are induced by the intraband Fröhlich interaction. The $F_{2g}+F_{1u}$(LO) combination is due to combined Fröhlich–deformation-potential interaction.

I. INTRODUCTION

Mg_2Si, Mg_2Ge, and Mg_2Sn are small-band-gap semiconductors and crystallize in the antifluorite structure (O_h point group). The primitive unit cell has inversion symmetry and contains three atoms: thus, there are two triply degenerate optical phonons at $\vec{q}=0$. One of them (F_{2g}) is even and Raman active, while the other (F_{1u}) is odd and infrared active. The macroscopic Coulomb field splits the F_{1u} mode into a doubly degenerate TO mode and a LO mode.

The phonon dispersion relations of these materials have been calculated by several workers[1-4] (see Fig. 1 for Mg_2Si), however, with the possible exception of Mg_2Sn which has been measured by neutron scattering,[4] there still is considerable ambiguity in the calculated dispersion relations. This is a result of the limited number of parameters available from experiment to obtain the force constants.

The first-order and some aspects of the second-order Raman spectra of these materials have already been reported.[5-11] However, all measurements were performed on cleaved (111) faces and no attempt was made to separate the three independent components of the Raman tensor (A_{1g}, E_g, and F_{2g} or $|a^2|$, $|b^2|$, and $|d^2|$, respectively, in Loudon's notation).

The band structure of these materials has also been calculated and compared with the results of optical measurements (see Fig. 2 for Mg_2Ge).[12-17] The materials are isoelectronic to germaniumlike semiconductors and, since they have the same translation lattice, their band structures are very similar. In particular, there are direct energy gaps E_0 and E_1 accessible to resonance experiments

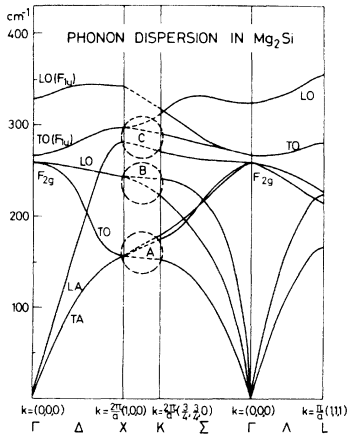

FIG. 1. Phonon dispersion curves of Mg_2Si (from Ref. 1). The encircled regions labeled A, B, and C, have been assigned to the broad density of states structures in the Raman spectra of Figs. 3 and 4.

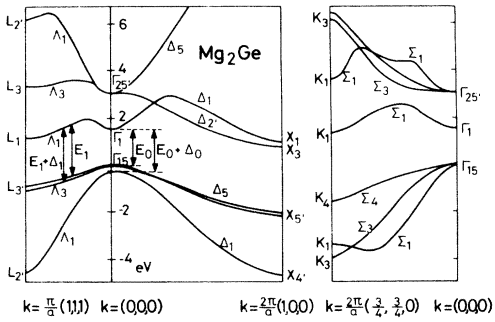

FIG. 2. Energy band structure of Mg_2Ge (from Ref. 14). The spin-orbit splitting of the valence bands has been schematically added.

with presently available discrete and tunable lasers. Some resonant scattering has already been investigated by using a few discrete lines of an Ar^+ laser.[7-11]

In this paper we present measurements on cleaved (111) and polished (100) faces of Mg_2Si, Mg_2Ge, and Mg_2Sn which yield the three independent components of the Raman tensor. By using a tunable cw dye laser and several gas lasers information on the resonant behavior of these spectra has been obtained in the region 1.83–2.81 eV, which covers the E_1 gap of Mg_2Ge (~2.5 eV), the E_0 (~2.2 eV) and E_1 (~2.6 eV) gaps of Mg_2Si, and the E_1 (~2.2 eV) and $X_{5'} \rightarrow X_1$ (~2.65 eV) gaps of Mg_2Sn (for a definition of these gaps see Fig. 2).

The resonance of the Raman allowed F_{2g} phonon for these three materials near the E_1 and $E_1 + \Delta_1$ gaps is well described by three-band terms in the dielectric theory of the Raman tensor. The small resonance intensity observed at this E_0 gap for Mg_2Si is interpreted as due to a small value of the deformation potential d_0 at this gap. Such a small value of d_0 is indeed calculated by the pseudopotential method and results from the small pseudopotential form factors of Mg. We have not performed calculations of the corresponding deformation potentials along the Λ direction. Such calculations are required to interpret in a quantitative fashion the ratio of the strengths of the E_0 and the E_1 resonances.

The sharp resonance of the Fröhlich-interaction-induced forbidden LO, its overtone 2LO, and the combination of $F_{1u}(\mathrm{LO}) + F_{2g}$ phonons at the E_1, $E_1 + \Delta_1$, and at the X gaps are shown to be well described by the square of the magnitude of the second derivative of the dielectric constants with respect to the incident photon energy; these resonances are strongly polarized in parallel-parallel scattering configurations.

The resonance in the X-gap region for Mg_2Sn is found to be analogous to that of the E_1 gap. The F_{2g} allowed phonon resonates broadly and weakly, however, Fröhlich-interaction-induced $F_{1u}(\mathrm{LO})$, its overtone and the combination of $F_{1u}(\mathrm{LO}) + F_{2g}$ resonate sharply and show a doublet structure due to the spin-orbit splitting of the $X_{5'}$ valence band.

The spin-orbit splittings observed in the resonances at E_1 gaps are 0.14 eV for Mg_2Ge and 0.27 eV for Mg_2Sn; at the X gap the splitting is 0.14 eV for Mg_2Sn.

The second-order Raman spectra of these materials are mainly Fröhlich-interaction-induced overtones or combinations of phonons with $\vec{q} \simeq 0$. However, we can observe a small structure in Mg_2Sn which resonates in the way that can be described by two-band terms in the dielectric theory of the Raman tensor. This second-order process seems to be of the type produced by the electron–two-phonon interaction in first order and therefore it is likely to be related to structure in the density of states at points near the edge of the Brillouin zone. We can also observe some second-order Raman bands due to the density of states in Mg_2Si, however, they resonate very weakly.

The deformation potentials involved in the several resonances observed are discussed and an attempt to determine their relative values is made. A preliminary report of this work was presented at the third International Conference on Light Scattering in Solids, in Campinas, Brazil.[18]

II. EXPERIMENT

The experiments were performed in the backscattering configuration on surfaces obtained from undoped ingots either by cleaving (111) surfaces or, in the case of (100) surfaces, by cutting, lapping, and polishing etching with Syton (Monsanto Chemical Co., St. Louis, Mo.). We used mainly (100) surfaces for Mg_2Si and (111) surfaces for Mg_2Ge and Mg_2Sn. After orientation with x rays, the polished (100) face was used to observe the $|d|^2$ component of the spectrum with incident and scattered polarizations parallel to [010] and [001], respectively. Polarizations parallel to [011] and $[01\bar{1}]$, respectively yielded $3|b|^2$, while both polarizations parallel to [010] yielded $|a|^2 + 4|b|^2$. From the cleaved (111) face $|a|^2 + |b|^2 + |d|^2$ and $|b|^2 + \frac{2}{3}|d|^2$ were obtained with incident and scattered polarizations parallel and perpendicular, respectively. The spectrometer was a standard double monochromator system with a spectral slit width of 7 cm^{-1} and detection by photon counting. The discrete lines of Kr^+, Ar^+, and He-Cd lasers were used, together with a cw tunable dye laser operated with rhodamine 6G. The laser radiation was focused on the sample with a cylindrical lens in order to prevent heating. The measurements were performed at 77 and 300 K for Mg_2Si but only at 77 K for Mg_2Ge and Mg_2Sn. While attempting to

measure Mg_2Ge at room temperature we had difficulties with surface deterioration when large laser powers were used. No such difficulties appeared when the samples were cooled down to 77 K.

The scattering intensities were normalized to those of a CaF_2 crystal so as to correct for laser intensity, monochromator transfer function, and ω^4 law. Because of the large band gap of CaF_2, its Raman tensor should be nondispersive in the region of interest to us. The frequency dependence of the light penetration depth was accounted for by multiplying the observed intensity by the sum of the absorption coefficients for the incident and the scattered radiation.[19]

III. RESULTS AND INTERPRETATION

As in germanium-type semiconductors,[20] the E_g component of the Raman tensor was found to be negligible for Mg_2Si, Mg_2Ge, and Mg_2Sn ($b \simeq 0$). We now proceed to discuss the results obtained for the three materials separately.

A. Mg_2Si

The $|a|^2+4|b|^2$ ($\simeq|a|^2$) and $|d|^2$ components of the Raman spectra of Mg_2Si for several exciting laser frequencies which cover the region of the E_0 and E_1 gaps are shown at room temperature in Figs. 3 and 4, respectively. The main structure is the first-order Raman-allowed F_{2g} phonon which

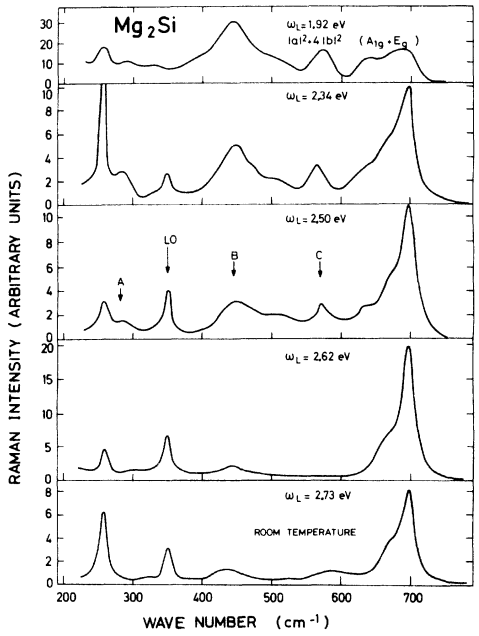

FIG. 3. First- and second-order Raman spectra corresponding to the sum of the $|a^2|$ and $4|b^2|$ components of Mg_2Si at room temperature for five scattering photon energies covering the E_0 and E_1 gaps.

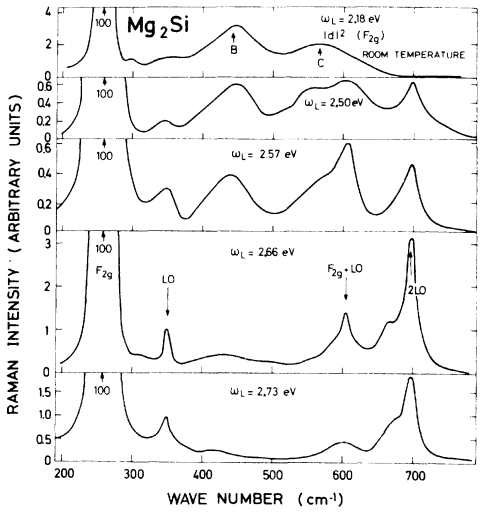

FIG. 4. $|d^2|$ component of the first- and second-order Raman spectra of Mg_2Si at room temperature for five scattering photon energies covering the E_0 and E_1 gaps. The "arbitrary" units of intensity are the same as for Fig. 3.

appears in the $|d|^2$ spectrum (Fig. 4), as required by group theory. The corresponding structure in the $|a^2|+4|b^2|$ spectrum (Fig. 3) is forbidden and hence relatively weak. It may be induced either by misorientations or by spatial dispersion.

We can see sharp peaks at 348 cm^{-1} and very close to the overtone of this energy (696 cm^{-1}). These peaks are particularly strong in the A_{1g} component. By comparison with the phonon dispersion curves,[1] they can be interpreted as due to the creation of F_{1u}(LO) phonons and their overtones, respectively. The F_{1u}(LO) phonon line is rather symmetric, however, its overtone 2LO has an asymmetric shape; two shoulders are seen in the lower-energy side of the main peak. These shoulders are likely to be 2LO overtones away from Γ, with contributions from the Σ-K-X line (see Fig. 1).

We can also see peaks in the $|d^2|$ spectra (Fig. 4) at 348 and 695 cm^{-1}, corresponding to F_{1u}(LO) and its overtone, respectively. They are, however, about ten times weaker than those observed in the $|a^2|$ spectra. Therefore, the Raman tensor of the F_{1u}(LO) peak and its overtone is mainly diagonal. We also observe a rather strong peak in the $|d^2|$ spectra at 607 cm^{-1}. This energy corresponds to the combination of F_{1u}(LO)+F_{2g} phonons; if this assignment is made, the structure at 607 cm^{-1} is parity forbidden. Correspondingly, the F_{1u}(LO) peak and the F_{1u}(LO)+F_{2g} combination structure resonate very sharply. The same is true of the F_{1u}(LO) overtone.

In addition to these prominent structures we can see some extra ones labeled A, B, and C in Figs.

3 and 4. The B and C bands are about six times stronger in the $|a^2|$ spectra than in the $|d^2|$ spectra.

The heights of the F_{2g} first-order Raman peak at 300 and 77 K are shown in Fig. 5 as a function of exciting laser energy, together with the function $|d\epsilon/d\omega|^2$ calculated from the data of Ref. 16 at 77 K. (ϵ is the dielectric constant.) This curve represents the scattering cross section for two-band processes under the assumption of a phonon frequency small compared with the lifetime of the corresponding electronic states. It should apply to the E_0 and E_1 gaps of Mg_2Si because of the small spin-orbit splitting ($\Delta_0 \simeq 0.03$ eV, $\Delta_1 \simeq 0.02$ eV) (see Sec. IV). The calculated E_1 resonance curve shows double peaks. The observed resonance curve shows also double peaks at 2.7 and 2.48 eV at 77 K, however the difference in the energy between the two peaks observed is larger than the calculated one. According to the calculated band structure the peak near 2.48 eV may correspond to the transition at the L point ($L_{3'} \rightarrow L_1$), while the main peak at 2.7 eV would be due to a region along Λ. The room-temperature resonance curve also exhibits a double peak which is rather similar to the theoretical curve.

The experimental curve of Fig. 5 shows a shoulder near the E_0 gap (~2.2 eV), while the corresponding peak in the theoretical curve is considerably stronger. In Fig. 6 the contribution of the E_0 gap to the Raman resonance, estimated by subtracting the E_1 background, is shown for the experimental (a) and for the theoretical (b) curves. Also, curve (c) in Fig. 6 corresponds to a calculation based on parabolic bands extending to infinity (see Sec. IV). The observed resonance peak is shifted by about 0.07 eV to higher energies with respect to the peak of the theoretical curve $|d\epsilon/d\omega|^2$.

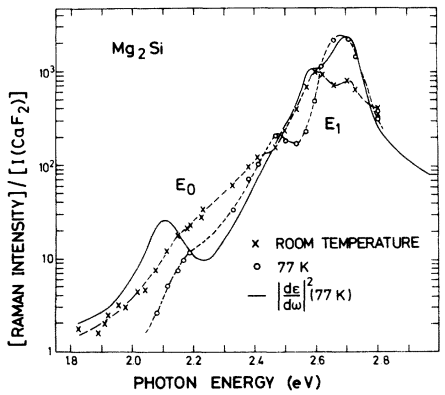

FIG. 5. First-order resonance of the F_{2g} phonon of Mg_2Si at room temperature (crosses) and at 77 K (circles). The solid line represents the function $|d\epsilon/d\omega|^2$ calculated from the data of Ref. 16 at 77 K. Structure is seen near the E_1 and E_0 band gaps.

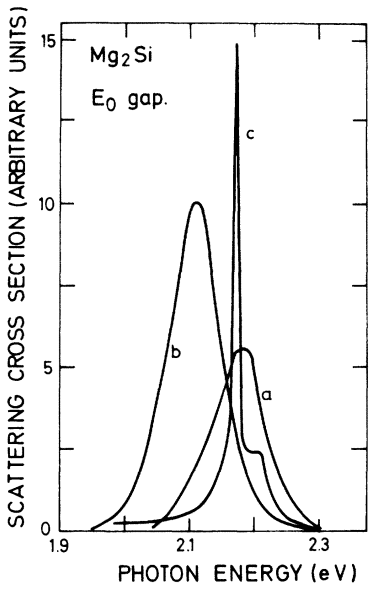

FIG. 6. First-order resonance of the F_{2g} phonon of Mg_2Si at 77 K near E_0 gap (a) obtained from the experimental data of Fig. 5 with the background due to E_1 subtracted. (b) Corresponding contribution of $|d\epsilon/d\omega|^2$ to the E_0 gap, also after subtracting the E_1 background. (c) Theoretical calculation performed with Eq. (3).

The resonance energy of the theoretical calculation based on parabolic bands was chosen to fit the observed resonance.

The half width of the curve $|d\epsilon/d\omega|^2$ is nearly the same as that of the observed resonance curve. The observed E_0 resonance is about two times weaker than that predicted on the basis of $|d\epsilon/d\omega|^2$ fitted to match the height of the E_1 resonance. This fact can be attributed to an electron-phonon interaction weaker at E_0 than at E_1. A preliminary calculation using the pseudopotential method yields a deformation potential $d_0 = 7.5$ eV, a rather small value when compared to that found for Ge (33 eV, see Appendix). This conclusion must, nevertheless, be regarded as tentative until a calculation of the corresponding deformation potential for the E_1 edge is performed.

In Fig. 7 the resonances of the forbidden first-order F_{1u}(LO) phonon and its overtone (2LO) are represented as found in the $|a^2|$ spectra, together with the curve $|d^2\epsilon/d\omega^2|^2$ based on the data of Ref. 16 at 77 K. The latter curve is expected to represent approximately the scattering cross section for a Fröhlich-interaction-induced LO (forbidden) and 2LO phonons[21]; the agreement with the experiment is good.

The resonances of the F_{1u}(LO) peak and its overtone (2LO) are very similar to each other, and about ten times stronger than that of the allowed F_{2g} phonon, also shown in Fig. 7.

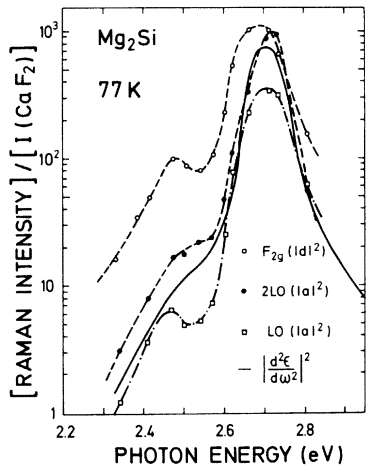

FIG. 7. Resonance of the F_{2g} phonon of Mg_2Si ($|d^2|$ component) at 77 K near the E_1 gap (open circles). Also, $|a^2|$ component of the resonance of the F_{1u}(LO) phonon (solid circles) and its overtone (open squares) near E_1 gap at 77 K for the same material. The solid line represents $|d^2\epsilon/d\omega^2|^2$ based on the data of Ref. 16 at 77 K.

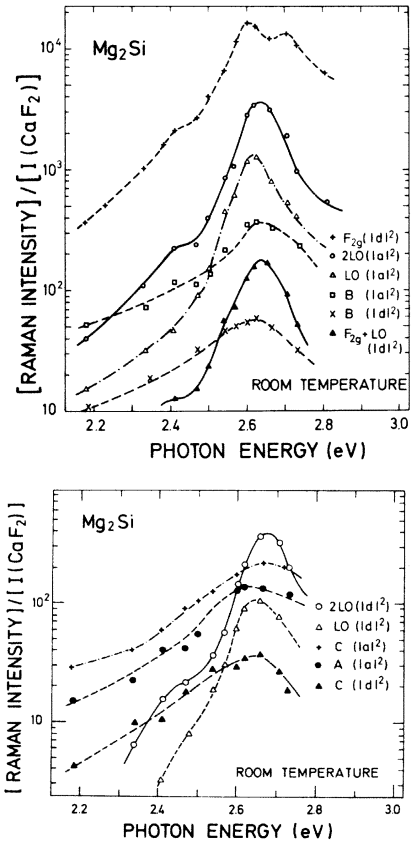

FIG. 8. First- and second-order Raman resonances of Mg_2Si at room temperature. The corresponding phonons and the Raman components for which the resonance was observed are listed in the figure. A, B, and C correspond to the same labels in Fig. 1, 3, and 4.

In Figs. 8(a) and 8(b) we have represented the resonance of the A, B, and C bands observed at room temperature, together with that of the F_{2g} + LO peak. As already mentioned the F_{2g}+ LO peak is only seen in the $|d^2|$ spectrum. Features B and C are observed in both the $|a^2|$ and $|d^2|$ spectra, while feature A in the $|d^2|$ spectrum is covered by the stronger F_{2g} allowed line. We also show in these figures, for comparison, the LO, 2LO, and F_{2g} resonances. The F_{2g}+ LO resonance is similar in shape to that of the LO and 2LO peaks in spite of the smaller overall strength. Peaks A, B, and C show an even weaker resonance than F_{2g} with the same shape in both $|a^2|$ and $|d^2|$ components. A comparison with Fig. 1 suggests that these peaks are due to overtones of the phonons in the corresponding encircled regions in the neighborhood of the X-K lines. The weak resonance of these structures can only be explained by assuming a nondispersive background to the Raman tensor, additive to the E_1 contribution, and related to virtual transitions at energies well above our experimental range. We have not seen any significant structure below that of the F_{2g} phonon.

B. Mg_2Ge

The $|a^2| + |b^2| + |d^2| \simeq |a^2| + |d^2|$ and $|d^2| + \frac{3}{2}|b^2| \simeq |d^2|$ components of the Raman spectra of Mg_2Ge at 77 K are shown in Figs. 9 and 10 for several laser frequencies in the region of the E_1 gap. In both figures the F_{2g} mode has been arbitrarily normalized to a height of 100.

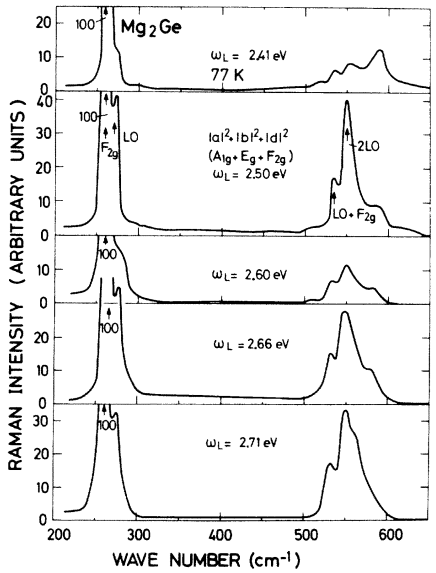

FIG. 9. First- and second-order Raman spectra of Mg_2Ge ($|a^2| + |b^2| + |d^2|$ components) at 77 K for five scattering photon energies in the neighborhood of the E_1 gap. The F_{2g} Raman-allowed phonon is normalized to 100.

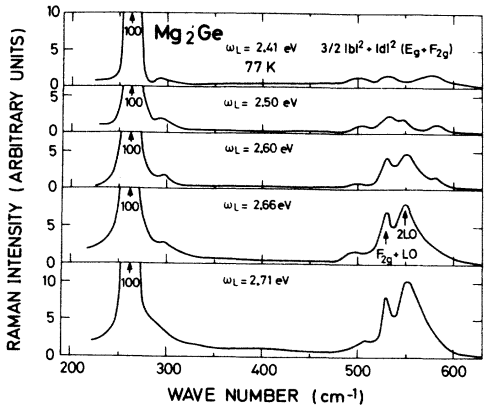

FIG. 10. First- and second-order Raman spectra of Mg_2Ge ($|d^2| + \frac{3}{2}|b^2|$ components) at 77 K for five scattering photon energies in the neighborhood of the E_1 gap. The F_{2g} Raman-allowed phonon is normalized to 100. The vertical scale is thus the same as that of Fig. 9.

The forbidden F_{1u}(LO) phonon and its overtone can be seen in the $|a^2|$ spectrum, as inferred from Figs. 9 and 10. The overtone also appears in the $|d^2|$ spectrum (Fig. 10), however, it is about ten times weaker than observed in the $|a^2|$ spectrum. The $|d^2|$ spectra show a $F_{1u}(\mathrm{LO}) + F_{2g}$ combination at 530 cm^{-1}. This is analogous to the case of Mg_2Si, nevertheless for Mg_2Ge the $\mathrm{LO} + F_{2g}$ combination also appears in the $|a^2|$ spectrum. The $\mathrm{LO} + F_{2g}$ phonon combination at the maximum of the resonance (see Fig. 11) is about four times larger in the $|a^2|$ than in the $|d^2|$ spectra.

Both $|a^2|$ and $|d^2|$ spectra have two faintly resonant structures at 590 and 513 cm^{-1}, which by comparison with the phonon dispersion curves of Ref. 2, could be assigned to 2LO overtones near the X and the L point of the Brillouin zone, respectively. We can also see a small structure near 295 cm^{-1} in the $|d^2|$ spectrum which could be due to the combination of TA + LA phonons.[2]

The resonances near the E_1 gap of the most prominent Raman structures observed for Mg_2Ge at 77 K are shown in Fig. 11. We find a situation rather similar to that found for Ge except for scattering involving polar LO-phonons, absent in Ge.[22] The LO, 2LO, and $\mathrm{LO} + F_{2g}$ phonons show in the $|a^2|$ spectra a doublet with a splitting of 0.14 eV which is near the expected spin-orbit splitting ($\Delta_1 \simeq 0.13$ eV) (Ref. 17) of the E_1 edge. The 2LO and $\mathrm{LO} + F_{2g}$ peaks in the $|d^2|$ spectrum show a broader resonance with a maximum between E_1 and $E_1 + \Delta_1$.

The Raman-allowed F_{2g} phonon also shows a broader peak between E_1 and $E_1 + \Delta_1$. The resonance of the first-order allowed F_{2g} mode is displayed in Fig. 12 together with the theoretical curve, $|(\epsilon^+ - \epsilon^-)/\Delta_1|^2$, which represents the resonance for a three-band process (see Sec. IV).[22]

The resonances of F_{1u}(LO) and its overtone in the $|a^2|$ spectrum near the E_1 gap at 77 K are shown in Fig. 13 together with the approximate theoretical curve $|d^2\epsilon/d\omega^2|^2$ based on the data of Ref. 16. This calculated curve represents the resonance for Fröhlich-interaction-induced or surface-field-induced normally forbidden LO phonon scattering.[21] The calculated curve has been shifted by 0.03 eV to higher energies in order to fit the observed resonance. This calculated curve shows well the double-peak structure due to spin-orbit interac-

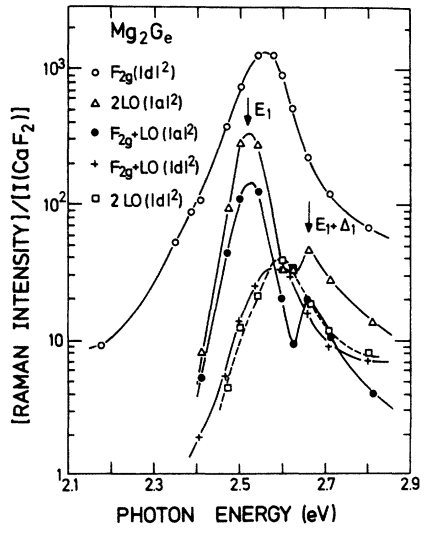

FIG. 11. First- and second-order resonances of Mg_2Ge at 77 K. The corresponding phonons and the Raman components for which the resonance was observed are listed in the figure. The arrows of E_1 and $E_1 + \Delta_1$ represent the estimated position of this spin-orbit-split gap.

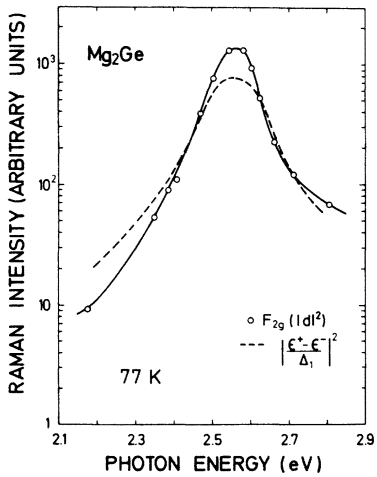

FIG. 12. First-order resonance of the F_{2g} phonon of Mg_2Ge at 77 K in the neighborhood of E_1 and $E_1 + \Delta_1$ gaps. The dashed line represents the theoretical calculation of the three-band term $|(\epsilon^+ - \epsilon^-)/\Delta_1|^2$ based on the data of Ref. 16 and the method of Ref. 26.

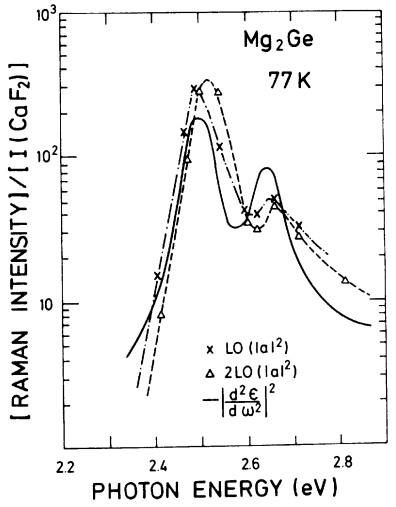

FIG. 13. First-order resonance of the forbidden F_{1u}(LO) and its overtones 2LO (both in the $|a^2|$ spectra) of Mg_2Ge at 77 K near E_1 and $E_1+\Delta_1$ gaps. Solid line is the theoretical calculation of $|d^2\epsilon/d\omega^2|^2$ based on the data of Ref. 16.

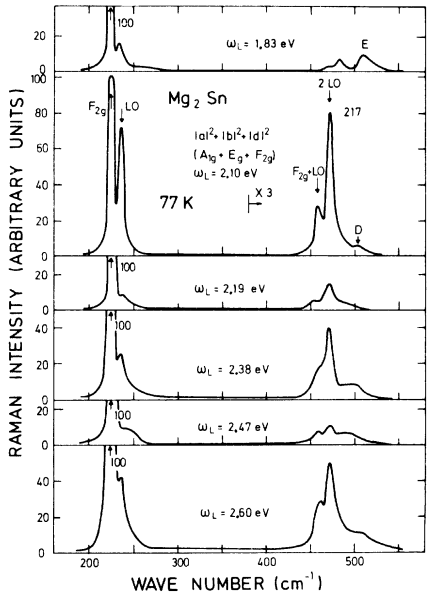

FIG. 14. First- and second-order Raman spectra of Mg_2Sn (sum of the $|a^2|$, $|b^2|$, and $|d^2|$ components) at 77 K for six scattering photon energies covering the E_1, $E_1+\Delta_1$, and the X-gap regions. The F_{2g}-allowed phonon is normalized to 100.

tion.

The resonance peak of the 2LO phonon, when plotted as a function of incident laser frequency, is 0.025 eV higher than that of the LO phonon. In the spirit of the quasistatic or adiabatic approximation one should actually plot the Raman intensities as a function of the average of the incident and scattered frequency ($\omega_L+\frac{1}{2}\Omega$ for Stokes scattering of frequency shift Ω). Thus 2LO is expected to peak $\Omega(\mathrm{LO})/2 \simeq 0.016$ eV above LO. The observed shift, 0.025 eV, is slightly higher than this value. A similar effect has been observed for the forbidden LO and the 2LO resonance in InSb.[23]

We do not see any structure in the Raman spectra of Mg_2Ge corresponding to the A, B, and C bands observed for Mg_2Si at room temperature. We note that it was also difficult to observe these bands for Mg_2Si at 77 K with laser frequencies higher than 2.4 eV.

C. Mg_2Sn

The sum of the $|a^2|+|b^2|+|d^2| \simeq |a^2|+|d^2|$ components of the Raman spectra of Mg_2Sn is shown in Fig. 14 at 77 K with exciting laser energies covering the region of the E_1 and $E_1+\Delta_1$ gaps, and the lowest direct gap at the X point of the Brillouin zone. The spectra are similar to those of Mg_2Ge. On the high-energy side of the Raman-allowed F_{2g} phonon the forbidden F_{1u}(LO) phonon appears, and at the 2LO energy a very sharply resonant peak is observed. At the low-energy side of 2LO a peak with an energy corresponding to the $F_{1u}(\mathrm{LO})+F_{2g}$ combination can be seen. For laser energies well below the E_1 gap, the bands on the higher-energy side of 2LO(Γ) become dominant compared with the 2LO peak which is dominant in the spectra near the E_1 gap and at higher energies. A comparison with the phonon dispersion relations of[3,4] Mg_2Sn suggests that the side bands D and E in Fig. 14 could be due to the 2LO overtone near the L and X points, respectively. The spectral shape of Mg_2Si near the 2LO(Γ) phonon is rather different from that of Mg_2Ge and Mg_2Sn. In the case of Mg_2Si the side bands appear at the low-energy side of 2LO(Γ). For Mg_2Ge and Mg_2Sn, however, sidebands appear at the high-energy side of the 2LO(Γ) peak. This is likely to be due to qualitative differences in the dispersion curve for LO phonons.

The F_{1u}(LO), its overtone, and the $F_{1u}(\mathrm{LO})+F_{2g}$ combination peak ($|a^2|$ component) resonate very sharply. The resonance of the forbidden F_{1u}(LO) and its overtone at 77 K ($|a^2|$ component) are shown in Fig. 15 together with the weaker allowed F_{2g} resonance ($|d^2|$ component). The theoretical expression for forbidden resonances $|d^2\epsilon/d\omega^2|^2$ calculated from the data of Ref. 16 at 77 K, is also represented in Fig. 15 (solid curve). As already mentioned, the curve $|d^2\epsilon/d\omega^2|^2$ is expected to represent approximately the resonance for Fröhlich-interaction-induced normally forbidden LO and for 2LO phonons.[21] The resonances of the LO and the 2LO phonons are qualitatively similar to this calculated curve (the measured E_1 peak is stronger than the calculated one) with a relative shift in energy of 0.04 eV. This shift can only be

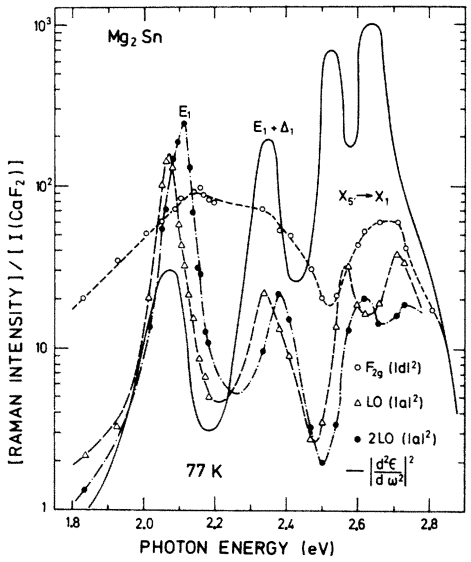

FIG. 15. First-order resonance of the Raman allowed F_{2g} phonon of Mg_2Sn ($|d^2|$ spectrum) at 77 K (open circles) together with the first-order resonance of the forbidden F_{1u}(LO) (Δ) and its overtone (solid circles) in the $|a^2|$ spectrum. The solid line represents $|d^2\epsilon/d\omega^2|^2$ calculated from the data of Ref. 16. In the $X_{5'} \rightarrow X_1$ gap region a spin-orbit splitting also seems to appear.

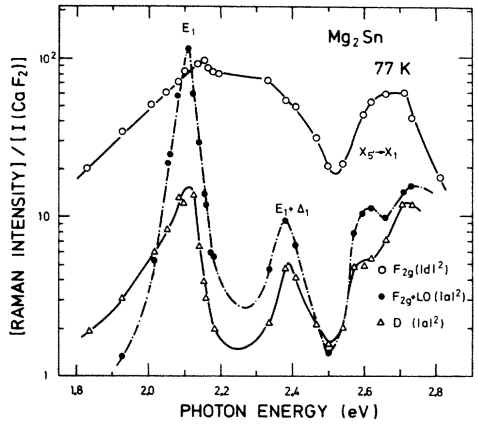

FIG. 16. Resonances of the combination of phonon of $F_{2g}+F_{1u}$(LO) for Mg_2Sn ($|a^2|$ component) and for the D band in Fig. 15 at 77 K. For comparison the resonance of the F_{2g} phonon is also represented.

partially accounted for in terms of the difference in the energy of the LO(Γ) and 2LO(Γ) excitations which would give a shift of 0.014 eV. The situation is similar to that described above for Mg_2Ge.

By comparison with LO and 2LO, the F_{2g} resonance is rather broad. Both the $|d^2\epsilon/d\omega^2|^2$ curve and the observed LO, 2LO, and LO+F_{2g} resonances exhibit peaks near 2.1, 2.35, 2.55, and 2.7 eV. The doublet at 2.07 and 2.34 eV for F_{1u}(LO), and at 2.11 and 2.38 eV for the 2LO peak corresponds to the E_1 and $E_1+\Delta_1$ gaps of Mg_2Sn, respectively. This doublet is analogous to that found for Mg_2Ge. Since the spin-orbit splitting Δ_1 of Mg_2Sn (0.28 eV) (Ref. 17) is larger than that of Mg_2Ge (0.13 eV), the doublet is better resolved in the resonance curve of Mg_2Sn than in that of Mg_2Ge.

In the higher-energy region above the E_1 and $E_1+\Delta_1$ gaps, we can also see a doublet resonance at 2.56 and 2.71 eV for the F_{1u}(LO) phonon and at 2.62–2.74 eV for the 2LO peaks. The resonance of the F_{2g} phonon shows a broad band with a suggestion of the doublet structure. We attribute this resonance to the lowest direct gap at $X(X_{5'} \rightarrow X_1)$ and the doublet to the spin orbit splitting of the $X_{5'}$ valence band (see Sec. IV).

The resonance of the phonon combination $F_{2g}+F_{1u}$(LO) and the side band D described in Fig. 14 are shown in Fig. 16 together with the resonance of the first-order F_{2g} phonon for comparison. The resonance of the F_{1u}(LO)+F_{2g} combination is very similar to that of the 2LO (Fig. 15) and shows the doublets in both E_1- and X-gap regions. The side band D may seem to resonate similarly to the 2LO and the F_{1u}(LO)+F_{2g} phonons; however, in the lower-energy side of the E_1 gap the resonance of the D band is not as sharp as that of the F_{1u}(LO) or F_{1u}(LO)+F_{2g} phonons. The $E_1, E_1+\Delta_1$ part of the D resonance in the $|a^2|$ spectrum agrees rather well with $|d\epsilon/d\omega|^2$ (for the sake of clarity in Fig. 16 this curve has been omitted), a fact similar to that observed for overtones of phonons with $k \neq 0$ in Ge. This result implies that the scattering mechanism is a two-band process induced by the electron–two-phonon interaction. The corresponding three-band process does not exist in the $|a^2|$ spectrum.

The resonance of the Raman-allowed F_{2g} phonon is shown in Fig. 17 together with the theoretical curve $|(\epsilon^+ - \epsilon^-)/\Delta_1|^2$ obtained from the data of Ref.

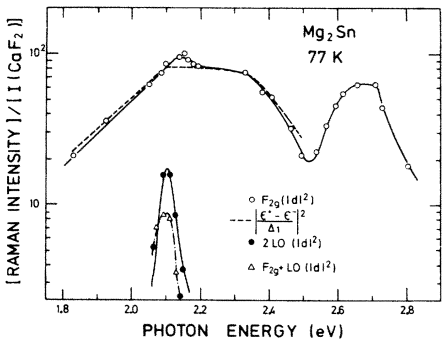

FIG. 17. Resonance of the first-order Raman-allowed F_{2g} phonon ($|d^2|$ component) of Mg_2Sn at 77 K. Dashed line is the theoretical calculation for three-band term $|(\epsilon^+ - \epsilon^-)/\Delta_1|^2$ based on the data of Ref. 16 and the method of Ref. 26. Open circles and triangles are, respectively, resonances of 2LO ($|d^2|$ spectrum) and $F_{2g}+F_{1u}$(LO) ($|d^2|$ spectrum) at 77 K.

16 at 77 K. This curve represents the resonance for the three-band model of the E_1 and $E_1+\Delta_1$ gaps (see Sec. IV). The agreement between the theory and the experiment is excellent and confirms that, as in the case of germanium, three-band processes dominate the F_{2g} resonance near the $E_1-E_1+\Delta_1$ gaps.

The resonances of the 2LO and the $F_{2g}+F_{1u}$(LO) phonons in the $|d^2|$ spectrum near the E_1 gap are shown also in Fig. 17. The 2LO phonon intensity in the $|d^2|$ component is about 20 times smaller than that in the $|a^2|$ component. Therefore, the Raman tensor for 2LO phonon scattering is mainly diagonal. The $F_{2g}+F_{1u}$(LO) combination peak in the $|d^2|$ spectrum has about $\frac{1}{10}$ the strength of the same combination in the $|a^2|$ spectrum.

IV. DISCUSSION

When the frequency Ω of the excitation created in the Raman process is negligible compared with the relevant electronic energies, the so-called dielectric, adiabatic, or quasistatic theory of the Raman tensor[24] can be used. More exactly, the condition of validity of the dielectric theory is $\Omega \ll |\omega_L-\omega_g+i\eta|$, where ω_L is the laser frequency, ω_g is the pertinent gap, and η is its lifetime broadening. In all cases treated here $\eta \gg \Omega$ and thus the dielectric theory is expected to apply.

The resonance of the first-order F_{2g} phonon near the E_1 and $E_1+\Delta_1$ gaps can be represented by the following formula for the Raman tensor[22] component d:

$$d=\frac{1}{4\pi}\left(\frac{2\sqrt{2}}{\sqrt{3}}\,\frac{\epsilon^+-\epsilon^-}{\Delta_1}d^5_{3,0}-\frac{1}{2\sqrt{3}}\frac{d\epsilon}{d\omega}d^5_{1,0}\right)\frac{\langle\xi^2\rangle^{1/2}}{a_0}\,, \tag{1}$$

where ϵ^+ and ϵ^-, which determined the three-band terms, are the contributions of the two gaps, E_1 and $E_1+\Delta_1$, to the dielectric constant ϵ, a_0 is the lattice constant, and ξ is the phonon amplitude. In Eq. (1), $d^5_{3,0}$ is a deformation potential which represents the coupling produced by the phonon between the spin-orbit-split Λ_3 valence bands. The deformation potential $d^5_{1,0}$ represents the splitting of the equivalent $\langle 111\rangle$ directions by the phonon. The first term in the right-hand side of Eq. (1) is produced by changes in the corresponding transition matrix elements. These matrix elements change, due to changes in the wave function produced by phonon-induced admixture of one of the two bands involved in the gap with a third band (three-band terms); in our case the mixing occurs between the two spin-orbit-split components of the valence band. The second term of Eq. (1) is due to phonon-induced variation in the energy gap between two bands (two-band terms). Equation (1) gives the sum of Stokes and anti-Stokes intensities. In order to obtain the usually measured Stokes intensity alone $\langle\xi^2\rangle$ must be replaced by n_B+1, with n_B the Bose-Einstein statistical factor for the corresponding phonons.

In the case of Mg_2Si, Δ_1 is very small (approximately 0.02 eV, thus $\Delta_1 \ll \eta$) and Eq. (1) reduced to the following expression[25]:

$$d=\frac{1}{4\pi}\sqrt{\tfrac{2}{3}}\left(d^5_{3,0}+\frac{1}{2\sqrt{2}}d^5_{1,0}\right)\frac{d\epsilon}{d\omega}\frac{\langle\xi^2\rangle^{1/2}}{a_0}\,, \tag{2}$$

where $d^5_{1,0}$ is probably negligible compared to $d^5_{3,0}$.[22] The Raman tensor component d is thus proportional to the derivative of the dielectric constant with respect to the photon frequency. This fact is used in Fig. 5; good agreement with the experiment is obtained.

The spin-orbit splitting of Mg_2Ge at the E_1 gap is approximately 0.14 eV and that of Mg_2Sn is approximately 0.27 eV, as obtained from Figs. 13 and 15. (We note that Δ_1 in Mg_2Ge fulfills the two-thirds rule: $\Delta_1 \simeq \frac{2}{3}\Delta_0$.)

Since the deformation potentials along the Λ direction of the Brillouin zone have not yet been calculated, we considered $d^5_{3,0}$ and $d^5_{1,0}$ as parameters and tried to find the appropriate ratio $d^5_{1,0}/d^5_{3,0}$ to fit the observed data. The agreement was best when we made $d^5_{1,0}$ equal to zero for both Mg_2Ge and Mg_2Sn; we thus conclude that three-band terms are indeed dominant at the E_1 and $E_1+\Delta_1$ gaps for the F_{2g} allowed phonon in these materials. The theoretical resonance curves thus obtained are represented in Figs. 12 and 17 for Mg_2Ge and Mg_2Sn, respectively; the agreement with the observed resonance is good.

Within the dielectric theory of the Raman tensor, and using the infinitely extended parabolic band model, the resonance of the first-order F_{2g} Raman tensor near the E_0 and $E_0+\Delta_0$ gaps is represented by the following formula[20]:

$$d=\frac{\sqrt{3}\,C_0 d_0}{16\pi\omega_0}\times\left\{-g(x_0)+\left(4\frac{\omega_0}{\Delta_0}\right)\left[f(x_0)-\left(\frac{\omega_0}{\omega_{0s}}\right)^{3/2}f(x_{0s})\right]\right\}\times\frac{\langle\xi^2\rangle^{1/2}}{a_0}\,, \tag{3}$$

where ω_0 is the frequency of the E_0 gap, Δ_0 is its spin-orbit splitting, $x_0=\omega/\omega_0$, $x_{0s}=\omega/(\omega_0+\Delta_0)$, and C_0 is a constant only weakly depending on parameters of the material and with values of the order of 1 in atomic units, a_0 is the lattice constant and d_0 is the deformation potential at E_0. The functions $f(x)$ and $g(x)$ are

$$g(x) = x^{-2}[2 - (1+x)^{-1/2} - (1-x)^{-1/2}], \quad (4)$$

$$f(x) = x^{-2}[2 - (1+x)^{1/2} - (1-x)^{1/2}]. \quad (5)$$

The resonance curve calculated with Eq. (3) is represented in Fig. 6 together with the observed E_0 resonance and the theoretical calculation $|d\epsilon/d\omega|^2$ based on the data in Ref. 16 with the background due to the E_1 edge subtracted. The theoretical calculation with Eq. (3) shows a peak at the E_0 gap sharper than those observed in Raman scattering and calculated from the experimental dielectric constant with $|d\epsilon/d\omega|^2$. Thus we conclude that the E_0 and $E_0+\Delta_0$ gaps are significantly broadened by lifetime effects. This may result from the fact that the $E_0 - E_0+\Delta_0$ direct gaps overlap a strong background of indirect transitions which start at the indirect gap of about 0.7 eV.[14]

The theory of the forbidden one-LO-phonon scattering has been discussed by a number of authors.[27-32] Since the forbidden scattering is much weaker for the TO phonon, the mechanism responsible for the violation of the selection rule must be related to a specific property of the longitudinal phonons, namely, to the electric field which accompanies them. This electric field can produce intraband scattering of electrons (Fröhlich interaction). A detailed calculation shows that the Raman tensor for this mechanism is mainly diagonal, and the "forbidden" nature of the effect is represented by a proportionality to the wave vector of the phonon $\vec{q}$. This "forbidden" nature is lifted if a surface electric field is present but the resulting selection rules are the same. The "forbidden" LO phonon observed in the $|a^2|$ component are for Mg_2Si, Mg_2Ge, and Mg_2Sn about ten times larger than those observed with crossed polarizations in the $|d^2|$ component.

As a "forbidden" process, the LO-forbidden scattering should resonate more sharply than the corresponding allowed processes. We may thus expect the leading term in the Raman tensor of the $\vec{q}$-induced or field-induced processes to be proportional to the derivative of the corresponding term in the allowed Raman tensor. This expectation is confirmed by a detailed calculation of the effect.[21] Thus, within the two-band model, the Raman tensor for the forbidden LO phonon can be represented by $d^2\epsilon/d\omega^2$. In Figs. 7, 12, and 15, the corresponding $|d^2\epsilon/d\omega^2|^2$, calculated on the basis of the data of Ref. 16, are shown for Mg_2Si, Mg_2Ge, and Mg_2Sn, respectively. The agreement with the observed resonance is good for Mg_2Si and Mg_2Ge. For Mg_2Sn the intensities of the observed E_1 and $E_1+\Delta_1$ peaks are reversed with respect to the calculated ones.

In our experiments we see a strong resonance of the structure which corresponds to the emission of two LO phonons with $\vec{k} \simeq 0$. One could, in this case, describe the "forbidden" scattering by one of the two phonons as induced by the electric field which accompanies the other LO phonon. Thus, the two-LO (Γ) process becomes allowed and is expected to have a resonance shape analogous to that of the forbidden scattering by single LO phonons. The observed 2LO phonons for Mg_2Si, Mg_2Ge, and Mg_2Sn do indeed resonate similarly to the LO phonons of the respective materials.

An analogous resonance has also been observed in the $|d^2|$ spectrum of a F_{2g}-plus-LO-phonon pair at Γ [Fig. 8(a)]. This resonance, about 15 times weaker than that of the two LO phonons in the case of Mg_2Si, must be attributed to a deformation-potential (F_{2g})–Fröhlich-interaction (LO) process, which becomes allowed because the relevant $\vec{q}$ is not the wave-vector transfer but the average k_1 of one of the contributing phonons.

In the case of Mg_2Sn, we can cover the energy range of the $X_5' - X_1$ gap[14] with our available lasers. (This gap is not to be taken literally to occur at the X point. The Δ_5, Δ_1, and Δ_2' bands, Fig. 2, are nearly parallel before reaching X.) As in the case of the $E_1 - E_1+\Delta_1$ edges a contribution from an extended region of the Brillouin zone may be important. The resonances in this range are quite similar to those in the region of the E_1 and $E_1+\Delta_1$ gaps. The F_{2g} Raman-allowed phonon resonates in one broad band. The Fröhlich-interaction-induced "forbidden" LO, 2LO, and LO+F_{2g} structures resonate more sharply and show doublets due to the spin-orbit splitting of the X_5' valence band. The observed splitting is about 0.14 eV. This value is smaller than the spin-orbit splitting Δ_1 of the valence band at a Λ point in the Brillouin zone (0.27 eV). The smaller spin-orbit splitting of the valence band at the X point compared with that at Λ may reflect a greater contribution of the Mg atom to the valence band at the X point. It is interesting to note that in germanium the admixture of Γ_{15} conduction-band wave function (corresponding in our case to Mg_{3p}) to the $\Gamma_{25'}$ conduction band is larger along Δ than along Λ,[33] in agreement with the present considerations. It may also be due to the averaging over an extended Δ region; the apparent spin-orbit splitting decreases in going from X_5' to Γ along Δ. To the best of our knowledge this constitutes the first determination of a splitting at an X_5' point in these compounds.

For Mg_2Si, $\Delta_0 \simeq 0$. In the limit $\Delta_0 \to 0$ Eq. (3) can be transformed into

$$d = \frac{\sqrt{3}\, d_0 \langle \xi^2 \rangle^{1/2}}{4\pi a_0} \frac{d\epsilon}{d\omega}, \quad (6)$$

where ϵ is the contribution of E_0 and $E_0+\Delta_0$ to the

dielectric constant. By using Eqs. (2) and (6) and the value of d_0 for Mg_2Si obtained in the Appendix, $d_0 = 7.5$ eV, and comparing the calculated expression $|d\epsilon/d\omega|^2$ with the observed E_0 and E_1 resonances we obtained the deformation potential at the E_1 gap. We found for Mg_2Si, $d^5_{3,0} + (1/2\sqrt{2})\, d^5_{1,0} = 26.6$ eV. This value is considerably larger than that of the E_0 gap. It is interesting to note that close to $k = 0$, $d^5_{3,0} \simeq \sqrt{2}\, d_0$ and $d^5_{1,0} \simeq d^{22}_0$. Thus $d^5_{3,0} + (1/2\sqrt{2})\, d^5_{1,0} \simeq 13.3$ eV, exactly a factor of 2 smaller than found experimentally. We thus conclude that either $d^5_{3,0} + (1/2\sqrt{2})\, d^5_{1,0}$ grows with increasing k along Λ, a fact which seems unlikely but should be verified by detailed calculations, or else there are inaccuracies either in the values of $\epsilon(\omega)$ used to calculate $d\epsilon/d\omega$ or in subtracting the large background of the E_0 resonance. This is not unlikely for the rather weak E_0 structure.

The Raman tensor (d) at the X gap is expressed for the case of zero spin-orbit splitting by[25]

$$d = \frac{1}{8\pi} d^t_{4,0} \frac{d\epsilon}{d\omega} \frac{\langle \xi^2 \rangle^{1/2}}{a_0}, \tag{7}$$

where $d^t_{4,0}$ is the corresponding intraband deformation potential at the X point.

The finite spin-orbit splitting makes the structure of the resonance more complicated for Mg_2Sn at the E_1 gaps and the X gaps. However, if we consider the lower tail of the E_1 gap and the higher tail of the X gap in the resonance, where the limit of zero spin-orbit splitting should apply, we can in a simple way obtain the ratio of the deformation potentials at the E_1 and X gaps: $(d^5_{3,0} + (1/2\sqrt{2}) \times d^5_{1,0})/d^t_{4,0} = 2.2$. Under the assumption that the deformation potential for the E_1 resonance is the same for Mg_2Sn as for Mg_2Si, namely, $d^5_{3,0} + (1/2\sqrt{2}) d^5_{1,0} = 26.6$ eV, we find the deformation potential $d^t_{4,0}$ to be 12.1 eV. We point out that, near $\vec{k} = 0$, $d^t_{4,0} \simeq \sqrt{3}\, d_0 = 12$ eV (taking for d_0 the value calculated in the Appendix, for Mg_2Sn, namely, $d_0 = 7.1$ eV) in rather good agreement with the value obtained from the analysis of the resonance curve.

We also performed measurements of the relative intensities at the E_1 resonance with cleaved surfaces and the same scattering configuration for the three materials. We found that the ratio of $d^5_{3,0}$ for Mg_2Ge to $(d^5_{3,0} + (1/2\sqrt{2}) d^5_{1,0})$ for Mg_2Si is 1.4 while the ratio of $d^5_{3,0}$ for Mg_2Sn to $(d^5_{3,0} + (1/2\sqrt{2}) \times d^5_{1,0})$ for Mg_2Si is 2.4. The contribution of the $d^5_{1,0}$ of Mg_2Si to these ratios can be safely neglected. In view of possible errors introduced in the measurement of the relative intensities by alignment difficulties and surface effects, we believe these results indicate that the $d^5_{3,0}$'s are similar in the three materials. The experimentally measured scattering intensities, however, are two orders of magnitude larger in Mg_2Si than in Mg_2Sn, a result of differences in the resonance functions $d\epsilon/d\omega$ and $(\epsilon^+ - \epsilon^-)/\Delta_1$ for these materials. We should finally point out that the cleaved Mg_2Sn surface was nearly perfect, while that of Mg_2Si contained a large number of steps, a fact which may account for the ratio of 2.4 obtained for the corresponding deformation potentials $d^5_{3,0}$.

ACKNOWLEDGMENTS

We would like to thank Professor E. Anastassakis for useful discussions and help at the earlier stage of this work. Thanks are also due to Dr. E. Schönherr for growing the crystals used in these experiments and to Dr. R. Zeyher for discussions concerning the theoretical aspects of this work.

APPENDIX

We calculated the first-order deformation potential of the valence band of Mg_2Si at the Γ point by using the pseudopotential method and perturbation theory. Restricting ourselves to plane waves with reciprocal-lattice vectors $(2\pi/a_0)|\vec{G}|$ with $|\vec{G}| = 3$ or 4, a procedure which is known to yield fairly accurate deformation potentials for Ge, the Γ_{15} valence bands are obtained by diagonalizing the following 2×2 matrix[24] (all energies are in rydbergs):

$$\begin{pmatrix} A & B \\ B & C \end{pmatrix},$$

where

$$\begin{aligned} A &= \frac{\Omega_{Si}}{\Omega_{cell}} (V^{Si}_4 - V^{Si}_{12} - V^{Si}_8) \\ &\quad + \frac{2\Omega_{Mg}}{\Omega_{cell}} (-V^{Mg}_4 - V^{Mg}_8 + V^{Mg}_{12}) + 3\left(\frac{2\pi}{a_0}\right)^2, \\ B &= (2\Omega_{Si}/\Omega_{cell})(V^{Si}_3 - V^{Si}_{11}), \\ C &= \frac{2\Omega_{Mg}}{\Omega_{cell}} (-V^{Mg}_{16}) + \frac{\Omega_{Si}}{\Omega_{cell}} (-V^{Si}_{16}) + 4\left(\frac{2\pi}{a_0}\right)^2. \end{aligned} \tag{A1}$$

In Eq. (A1), Ω_{cell} is the volume of the unit cell of Mg_2Si, while Ω_{Si} and Ω_{Mg} represent the volume per atom in crystalline Si and Mg, respectively.

The x component of the associated eigenvectors has the form

$$\Gamma_{15,X} = \alpha [111]_{15,X} + \beta [200]_{15,X},$$

where $[ijk]_{15,X}$ denotes the appropriately symmetrized linear combinations of equivalent plane waves with wave vector $\vec{G} = (2\pi/a)(i,j,k)$. Using the pseudopotential form factors of Ref. 34, one obtains for Mg_2Si, $\alpha = 0.88$ and $\beta = 0.47$. The deformation potentials for optical phonons give the splitting of the valence bands due to the sublattice shift $\vec{\tau} = (\frac{1}{4}a_0)(1+\delta, 1+\delta, 1+\delta)$. For $\delta \neq 0$, the Γ_{15} representation splits into a L_1^- and L_3^- representation. The function $\Gamma_{15,\bar{X}} = (1/\sqrt{2})(\Gamma_{15,X} - \Gamma_{15,Y})$

belongs to the L_3^- representation. From its shift with δ we can calculate the deformation potential d_0:

$$d_0 = \frac{4}{\sqrt{3}} \langle \Gamma_{15,\bar{x}} | \frac{dV}{d\delta} | \Gamma_{15,\bar{x}} \rangle$$

$$= -\frac{16}{\sqrt{3}} \pi\alpha\beta \frac{\Omega_{Mg}}{\Omega_{cell}} (V_3^{Mg} - V_{11}^{Mg}) . \quad \text{(A2)}$$

This deformation potential depends only on the pseudopotential form factors of Mg.

For a Ge-type material we have, instead of Eq. (A2),[24]

$$d_0 = -(4\pi/\sqrt{3})[\beta^2(V_4 - V_{12}) + \sqrt{2}\beta\alpha(V_3 - V_{11})] , \quad \text{(A3)}$$

and one obtains with the pseudopotential factors of Cohen and Bergstresser,[35] $d_0 \simeq 33$ eV for Ge. By replacing in Eq. (A2), the pseudopotential factors $V_3^{Mg} = -0.08$ and $V_{11}^{Mg} = +0.045$ Ry, considerably smaller than those of crystalline Ge($V_3 = -0.23$, $V_{11} = +0.06$ Ry), we find $d_0 = 7.5$ eV, correspondingly smaller than the Ge value. Following the same procedure, we obtained $d_0 = 7.1$ eV for both Mg_2Ge and Mg_2Sn.

---

*On leave from the Institute for Optical Research Kyoiku University, Sinzyuku-ku, Tokyo, Japan.

[1]W. B. Whitten, P. L. Chung, and G. C. Danielson, J. Phys. Chem. Solids 26, 49 (1965).
[2]P. L. Chung, W. B. Whitten, and G. C. Danielson, J. Phys. Chem. Solids 26, 1753 (1965).
[3]L. C. Davis, W. B. Whitten, and G. C. Danielson, J. Phys. Chem. Solids 28, 439 (1967).
[4]R. J. Kearney, T. G. Worlton, and R. E. Schmunk, J. Phys. Chem. Solids 31, 1085 (1970).
[5]L. Laughman and L. W. Davis, Solid State Commun. 9, 497 (1971).
[6]C. J. Buchenauer and M. Cardona, Phys. Rev. B 3, 2504 (1971).
[7]E. Anastassakis and C. H. Perry, in *Light Scattering in Solids*, edited by M. Balkanski (Flammarion, Paris, 1971), p. 47.
[8]E. Anastassakis and E. Burstein, in Ref. 7, p. 52.
[9]E. Anastassakis and C. H. Perry, Solid State Commun. 9, 407 (1971).
[10]E. Anastassakis and C. H. Perry, Phys. Rev. B 4, 1251 (1971).
[11]E. Anastassakis and E. Burstein, Solid State Commun. 9, 1525 (1971).
[12]P. M. Lee, Phys. Rev. 135, A1110 (1964).
[13]N. O. Folland, Phys. Rev. 158, 764 (1967).
[14]M. Y. Au-Yang and M. L. Cohen, Solid State Commun. 6, 855 (1968); and Phys. Rev. 178, 1358 (1969).
[15]F. Aymerich and G. Mula, Phys. Status Solidi 42, 697 (1970).
[16]W. J. Scouler, Phys. Rev. 178, 1353 (1969).
[17]F. Vázquez, R. A. Forman, and M. Cardona, Phys. Rev. 176, 905 (1968).
[18]S. Onari, E. Anastassakis, and M. Cardona, in *Light Scattering in Solids*, edited by M. Balkanski *et al.* (Flammarion, Paris, 1975), p. 54.
[19]R. Loudon, J. Phys. (Paris) 26, 677 (1965).
[20]B. A. Weinstein and M. Cardona, Phys. Rev. B 8, 2795 (1973).
[21]R. Zeyher (private communication).
[22]M. A. Renucci, J. B. Renucci, R. Zeyher, and M. Cardona, Phys. Rev. B 10, 4309 (1974).
[23]W. Kiefer, W. Richter, and M. Cardona, Phys. Rev. B 12, 2346 (1975).
[24]M. Cardona, *Atomic Structure and Properties of Solids*, edited by E. Burstein (Academic, New York, 1972), p. 514.
[25]J. B. Renucci, R. N. Tyte, and M. Cardona, Phys. Rev. B 11, 3885 (1975).
[26]D. D. Sell and E. O. Kane, Phys. Rev. 185, 1103 (1969).
[27]D. C. Hamilton, Phys. Rev. 188, 1221 (1969).
[28]R. Martin, Phys. Rev. B 4, 3676 (1971).
[29]J. G. Gay, J. D. Dow, E. Burstein, and A. Pinczuk, Ref. 7, p. 33.
[30]B. Bendow, J. L. Birman, A. K. Ganguly, T. C. Damen, R. C. C. Leite, and J. F. Scott, Opt. Commun. 1, 267 (1970).
[31]R. Zeyher, C. S. Ting, and J. L. Birman, Phys. Rev. B 4, 1725 (1974).
[32]R. M. Martin and T. C. Damen, Phys. Rev. Lett. 26, 86 (1971).
[33]M. Cardona and F. H. Pollak, Phys. Rev. 142, 530 (1966).
[34]A. O. E. Animalu and V. Heine, Philos. Mag. 12, 1249 (1965).
[35]M. L. Cohen and T. K. Bergstresser, Phys. Rev. 141, 789 (1966).